1977

Local buckling tests on two high-strength steel tubular columns, M.S. thesis, December 1977

Marc Anthony Marzullo

LOCAL BUCKLING TESTS ON TWO HIGH-STRENGTH STEEL TUBULAR COLUMNS

by

Marc Anthony Marzullo

A THESIS

Presented to the Graduate Committee

of Lehigh University

in Candidacy for the Degree of

Master of Science

in

Civil Engineering

Lehigh University

December 1977

This thesis is accepted and approved in partial fulfillment of the requirements for the degree of Master of Science.

Dec. 13, 1977
(date)

Professor Alexis Ostapenko
Professor in Charge

Professor David A. VanHorn
Chairman, Department of
Civil Engineering

ACKNOWLEDGEMENTS

The research reported was conducted at Fritz Engineering Laboratory, Lehigh University, Bethlehem, Pennsylvania. Dr. Lynn S. Beedle is Director of Fritz Laboratory and Dr. David A. VanHorn is Chairman of the Department of Civil Engineering. This investigation is part of a research project on local buckling of high-strength steel tubular columns sponsored by the American Iron and Steel Institute and conducted under the general guidance of a Task Force chaired by Mr. Robert R. Gavin.

The author wishes to gratefully acknowledge the help of Dr. Alexis Ostapenko, his thesis advisor, who devoted a considerable amount of time and effort in making pertinent comments and suggestions concerning the author's work.

Sincere gratitude is expressed to Stephen X. Gunzelman, a former graduate student of Lehigh University and coauthor of References 5 and 6, for his assistance with the author's first test and to Hamid Malekzadeh who assisted in the second test and helped in reducing experimental data. Special thanks are due to Kenneth R. Harpel, Robert R. Dales, Russell C. Longenbach, and the rest of the Laboratory's technical staff who helped in setting up and running the tests.

Finally, sincere thanks are due to the various support personnel in Fritz Engineering Laboratory. Ms. Shirley M. Matlock was responsible for typing the manuscript. Mr. John M. Gera, assisted by Mrs. Sharon D. Balogh and Mr. Richard W. Troxell, drafted the graphs and figures. Mr. Richard N. Sopko provided the required photographs.

TABLE OF CONTENTS

LIST OF TABLES

LIST OF FIGURES

ABSTRACT

Local buckling tests were conducted on two short tubular specimens fabricated from high-strength steel plate by cold-rolling and welding. One specimen had a transverse weld at midheight and was made from 345 MPa (50 ksi) nominal yield stress steel. It buckled at a stress equal to 0.872 F_y. The other specimen was made from 690 MPa (100 ksi) nominal yield stress steel and it buckled at a stress of 0.912 F_y. The diameter was 1.53 m (60 in.) for both specimens and the wall thickness was 7.26 mm (0.286 in.) for one and 6.55 mm (0.258 in.) for the second. The corresponding D/t ratios were 210 and 233.

The test results of the first specimen indicate that the presence of a transverse weld had no apparent effect on the intensity of the buckling stress although the initial buckling occurred at the weld seam. The buckling stress value of this specimen when plotted against geometric and material properties fell on a smooth curve formed by the test results of other specimens fabricated from 345 MPa (50 ksi) steel which had been tested previously at Lehigh University.

The test results of the second specimen which had a nominal yield stress twice the value of the first specimen indicate that the yield stress has a different effect on the local buckling stress above the proportional limit than is currently accepted.

Both tests substantiate the conservatism of the present API and AISI rules for local buckling of tubular columns.

1. INTRODUCTION

Tubular columns fabricated from high-strength steels by cold-rolling and welding are used in many engineering structures. Of particular interest are the columns in which local buckling is expected at stresses between the proportional limit and the yield stress. In this stress range, the design of fabricated members with respect to local buckling is handicapped by the discrepancies between the current design recommendations. The apparent cause of these discrepancies appears to have resulted from the sparcity and wide scatter of experimental data.

1.1 Current Design Rules

The principal design curves currently used to predict local buckling stress of fabricated tubular members are shown in Fig. 1: AISI (American Iron and Steel Institute) (1), API (American Petroleum Institute) (2), DNV (Det Norske Veritas, 1974) (8), Donnell & Wan (4), and Plantema (7). The ordinate is the ratio of the buckling stress to the yield stress and the abscissa is the nondimensional parameter α defined by

$$\alpha = \frac{Et}{F_y D} \tag{1}$$

where E is the modulus of elasticity, t is the wall thickness, F_y is the yield stress of steel, and D is the diameter.

There is substantial disagreement between many of these design curves. For example, the allowable stress values obtained from the API

and AISI curves, which are both recommended for the design of fabricated members in this country, are 151 MPa (22 ksi) and 255 MPa (37 ksi) for $\alpha = 2.3$.

1.2 Previous Experimental Research

There has been very little experimental research conducted on the inelastic local buckling of tubular columns fabricated from high-strength steel.

Tests on specimens fabricated from mild steels were conducted at the University of Illinois by Wilson and Newmark (9,10). The D/t ratio ranged from 69 to 320 and the thickness from 0.8 mm (0.031 in.) to 12.55 mm (0.494 in.). The yield stress varied from 213.8 MPa (31.0 ksi) to 279.3 MPa (40.5 ksi). The test points are shown by hollow circles in Fig. 1. The substantial scatter between the test results cannot be readily explained although Wilson and Newmark observed that at the same value of α, thicker tubes tended to develop a higher buckling stress than did the thinner tubes. They attributed this to greater geometric imperfections in the thinner tubes, but they did not quantitatively substantiate this conclusion.

In an experimental study of inelastic local buckling at Lehigh University, eight tests were conducted on tubular columns fabricated from the nominal 345 MPa (50 ksi) steel by cold-rolling and welding (5,6). The dimensions and material properties for these specimens are listed as P1 to P7 in Table 1. The actual yield stress varied from 319 MPa (46 ksi) to 377 MPa (54 ksi). The D/t ratios varied from 84.8 to 248.4

and the wall thickness from 7.26 mm (0.286 in.) to 8.35 mm (0.328 in.). The specimens were short with lengths from 2.03 m (80 in.) to 3.05 m (120 in.).

The test points, labeled P1 to P7, are shown by solid circles in Fig. 1. The points are very consistent among themselves as indicated by the fact that they form a continuous curve with very little scatter. The test values lie above all the other test points and design curves, thus indicating that for tubular columns fabricated from nominal 345 MPa (50 ksi) steel, the principal American design curves are quite conservative.

However, no general design recommendations can be made on the basis of these test results without additional research. The effect of different yield stress levels other than 345 MPa (50 ksi) must be investigated.

1.3 Present Research

The research described here explored the effect of a transverse weld and the effect of a higher yield stress steel on the intensity of the local buckling stress. Two specimens were tested. One specimen was fabricated from 345 MPa (50 ksi) steel and had a transverse weld located at midheight. The other specimen was fabricated from 690 MPa (100 ksi) steel. Each specimen failed by local buckling at a buckling stress above the proportional limit.

2. DESCRIPTION OF TEST SPECIMENS

2.1 Geometric Characteristics

The specimens tested in this program, P8 and P9, together with the pertinent notation are shown in Fig. 2. The dimensions and other data for the specimens are listed in Table 1 under labels P8 and P9. The outside diameter was 1.53 m (60 in.) for both specimens and the wall thickness was 7.26 mm (0.286 in.) for specimen P8 and 6.55 (0.258 in.) for specimen P9. The corresponding D/t ratios were 210 and 233. The values of parameter α were 2.60 and 1.40. The specimens had a length of 2.44 m (96 in.) and thus, they were short enough to exclude the effect of overall column buckling (L/r = 3.18). In order to achieve uniform distribution of the axial load, the specimens had an end ring, measuring 127 mm (5 in.) in width and 25.4 mm (1 in.) in thickness, welded to the ends of the specimens as shown in Fig. 2.

2.2 Material Properties

The average static yield stress determined at zero strain rate is listed in Table 1 for each specimen. The values for specimens P8 and P9, 372.0 MPa (53.96 ksi) and 622.76 MPa (90.32 ksi), were obtained from four tensile coupons. The coupons of the standard 203.2 mm (8 in.) gage length were fabricated in accordance with ASTM Standards (3) from the material sheared from the original flat plates. The properties of each coupon together with the averages are listed in Table 2.

2.3 Fabrication of Specimens

2.3.1 Specimen P8

Test specimen P8 was made by modifying the previously tested specimen P6. (The test on specimen P6 is described in Ref. 6.) First, the buckled portion at the top of specimen P6 was removed and the end ring was rewelded. The specimen was then flame cut at a height of 1.01 m (40 in.) separating the specimen into two sections. The top section was rotated counterclockwise 120^{o}, offsetting the longitudinal weld seams one third the circumference, and the two sections were rewelding into one unit as is shown in Fig. 3 on the left. Alignment of the specimen walls prior to rewelding was provided by special guides circumferencially located along the specimen wall. In the process of the modification, the length was reduced from the original 3.03 m (120 in.) of P6 to 2.42 m (96 in.) while all other dimensions (D,t) remained unchanged.

2.3.2 Specimen P9

Specimen P9 was fabricated from a flat plate by cold rolling it in a pyramid three-roll plate bending machine and welding the longitudinal seam. A submerged arc multi-pass vee weld was used for the longitudinal seam. A steel end ring was then welded to each end of the specimen. The completed specimen is shown in Fig. 2 on the right.

3. IMPERFECTIONS OF SPECIMENS

Geometric imperfections in the specimens were described by out-of-roundness, out-of-straightness, and local deviations. The out-of-roundness at any cross section is defined by the ASTM Standard (3) as

$$\text{Out-of-Roundness} = \frac{OD_{max} - OD_{min}}{OD} \tag{2}$$

where OD_{max}, OD_{min}, and OD are the maximum, minimum, and mean outside diameters, respectively. The maximum out-of-roundness was found to be at the bottom end of both specimens with the value of 0.0036 for specimen P8 and 0.0046 for specimen P9.

Out-of-straightness is defined as the maximum offset within a 1.52 m (5 ft) length between a longitudinal straight line and the specimen wall. The maximum out-of-straightness values were 5.9 mm (0.232 in.) for specimen P8 and 2.19 mm (0.0863 in.) for specimen P9. In both specimens, the maximum out-of-straightness was adjacent to the longitudinal weld seam.

Local deviations can be of three basic types; dents, gouges, and misalignment of the wall at weld seams. The interior and exterior walls and the weld seams were inspected, and no local deviations were found to warrant exact measurements except in specimen P8 at the transverse weld. Measurements were taken with a depth gage to determine the offset between the specimen wall across the transverse weld. The maximum offset, 4.36 mm (0.171 in.) was measured adjacent to the longitudinal weld which coincided with the location of the maximum out-of-straightness value.

The American Petroleum Institute (API) has set standards for the allowable out-of-roundness and out-of-straightness for tubular members (2). The maximum out-of-roundness shall satisfy the following two requirements:

$$\text{Out-of-Roundness} \leq \frac{0.25}{OD} \tag{3}$$

and

$$\text{Out-of-Roundness} \leq 0.01 \tag{4}$$

where OD is the mean outside diameter measured in inches. The allowable out-of-roundness value was 0.0041 for both specimens P8 and P9. Thus, only specimen P9, which had a maximum out-of-roundness value of 0.0046, slightly exceeded the API limit.

The maximum out-of-straightness allowed by the API standard is 1.58 mm (1/16 in.) in any 1.52 m (5 ft.) or 3.175 mm (1/8 in.) in any 3.05 m (10 ft.). The maximum out-of-straightness values of specimens P8 (5.9 mm) and P9 (2.19 mm) exceeded the 1.58 mm (1/16 in.) in 1.52 m (5 ft) limit.

In comparison to specimen P6 from which specimen P8 was made, the maximum out-of-straightness value increased from 1.0 mm (0.038 in.) to 5.9 mm (0.232 in.) and the maximum out-of-roundness decreased slightly from 0.0053 to 0.0036.

4. TEST SETUP AND INSTRUMENTATION

4.1 Test Setup

The test setup used for the two specimens is shown in Fig. 3. The specimen sits on the machine floor and is compressed from above with the loading head. The end ring at each end of the specimen distributes the load thus reducing the pressure on the machine surfaces. A layer of grout fills the gap between the end ring and the machine floor and head to ensure uniform load distribution.

Specimen P9 is shown in the testing machine completely instrumented and ready for testing in Fig. 4. The surface of the specimen was whitewashed to accentuate the regions of local yielding during the test. The grid lines designating the location of the lateral displacement measurements were scribed on the surface of the specimen and are shown numbered sequentially.

4.2 Instrumentation

The instrumentation used to measure longitudinal deformations consisted of mechanical dial gages and electrical strain gages. Four mechanical dial gages (0.001 in. accuracy) located beneath the corners of the machine head were used to measure longitudinal deformation of the specimen. Three electrical strain gages, cemented at third points along the circumference, gave readings of longitudinal strain in the specimen wall at midheight. These strains served to verify concentric loading of the specimen and provided an alternate means of measuring longitudinal deformations.

Lateral displacements of the specimen wall relative to the ends of the specimen were measured along each grid line with a movable dial gage rig. The rig, shown in Fig. 4 on the right side of the specimen, consisted of eight mechanical dial gages attached to a lightweight aluminum frame. The base of the rig rested on the bottom end ring of the specimen and the top of the rig was held against the specimen wall by an electromagnet.

Additional lateral displacements were made for some buckles by placing a straight edge against the specimen wall and measuring the offsets with a depth gage.

5. TEST PROCEDURE

5.1 Alignment

The test procedure was the same for both specimens and it consisted of the alignment and loading phases.

Alignment of the specimens in the testing machine was required to ensure concentric loading. This was achieved through a combination of tilting the loading head of the testing machine and grouting the contact surfaces between the end rings and the testing machine with Hydro-Stone* cement.

The first step was to apply a 13 mm (½ in.) layer of cement on the machine floor. The specimen was lowered on top of the cement and spread it to fill all the gaps between the machine floor and the end ring. The machine head was then tilted until a uniform gap existed between the top end ring and the machine head. A 13 mm (½ in.) layer of cement was then placed on the top end ring and the machine head was lowered onto it until the cement was squeezed to a minimum thickness of 6 mm (¼ in.). After hardening overnight, the cement provided a strong medium through which the load could be uniformly applied. The alignment of the specimen was later verified during the test by measuring longitudinal strains at the three mid-height locations around the circumference

Following the alignment, the instrumentation of the specimen was completed by attaching the four longitudinal dial gages between the floor and the machine head.

*Hydro-Stone cement manufactured by United States Gypsum Company. The mixture used was 32 parts water to 100 parts Hydro-Stone cement.

5.2 Test Sequence

The test began with a load of approximately 4.5 kN (20 kips) which was needed during the alignment. A complete set of readings of longitudinal deformation, lateral displacement, and longitudinal strains was recorded as the initial set of readings. The load was increased, at first in increments of 22.5 kN (100 kips) at a loading rate of 11.25 kN (50 kips) per minute until linearity was achieved on the load vs. axial deformation curve. Then, the load increments of 45 kN (200 kips) were used until buckling took place. Following the initial buckling, the specimens were loaded so that the longitudinal deformation was at a rate of 6.4 mm ($\frac{1}{4}$ in.) per minute. This rate allowed ample time to record the longitudinal dial gage readings without stopping the test except for resetting the dial gages after each 25 mm (1.0 in.) of axial deformation.

Longitudinal deformations were recorded at each load increment throughout the test. Longitudinal strains were recorded only up to the initial buckling. Lateral displacements of the specimen wall were recorded at the initial load and at several subsequent loads during the test.

6. GENERAL SPECIMEN BEHAVIOR

6.1 Behavior Prior to Buckling

The load-deformation curves of the two specimens for the range before buckling and immediately after buckling are shown in Fig. 5. The ordinate gives the load as a nondimensionalized ratio of the axial stress to the static yield stress and the abscissa is the longitudinal shortening.

The curves show, that after some initial nonlinearity, a linearly elastic load-deformation relationship existed essentially up to the point of buckling. The curve for specimen P8 shows a deviation from linearity in the last load increment prior to buckling whereas for specimen P9 the curve appears to deviate from linearity at approximately 0.675 F_y.

Local yielding was observed in specimen P8 at approximately 0.6 F_y. The yielding, indicated by the flaking off of whitewash was concentrated in two areas, along the transverse weld on one side and at the bottom of the specimen adjacent to the end ring on the opposite side. Later in the test, buckles developed in these areas. However, no flaking of the whitewash was observed in specimen P9 up to the point of buckling.

6.2 Behavior at Buckling

The failure of both specimens resulted from local buckling. The maximum value of average stress attained was 0.872 F_y for specimen P8 and 0.912 F_y for specimen P9. The corresponding longitudinal deformations were 4.97×10^{-3} m (0.196 in.) and 8.38×10^{-3} m (0.33 in.).

Initial buckling of specimen P8 occurred in the form of lobular buckles developing simultaneously in two distinct regions, one set along the transverse weld and the other set on the opposite side of the specimen adjacent to the bottom end ring. Together, these two levels of buckles encompassed the full circumference of the specimen.

The six lobular buckles which initially formed along the transverse weld extended approximately two-thirds the circumference as shown in Fig. 6. The pattern of buckles alternated above and below the weld with all the lobes protruding inward. Measurements of the length and amplitude of the initial buckles were taken after the load stabilized at 0.37 F_y. The length of the lobes ranged from 0.68 m (2.23 ft) to 0.8 m (2.62 ft). The amplitude of these buckles varied from 36.8 mm (1.45 in.) to 95.2 mm (3.75 in.).

The three lobular buckles which formed 0.2 m (8 in.) from the bottom of the specimen are shown in Fig. 7. These buckles extended approximately one-third the circumference of the specimen. The length of the buckles ranged from 0.63 m (2.06 ft) to 0.81 m (2.65 ft) and the amplitude from 57.1 mm (2.25 in.) to 76.2 mm (3 in.).

Initial buckling of specimen P9 was accompanied by an explosive sound while simultaneously, seven lobular buckles formed 0.241 m (9.5 in.) from the top of the specimen. Figure 8 shows the three inward lobular buckles between grid lines 8 and 13. The other four buckles were similar in appearance. After the load stabilized at 0.23 F_y, the length of the lobes varied from a maximum value of 0.76 m (30 in.) for the buckle adjacent to the longitudinal weld to a minimum value of 0.58 m (23 in.)

for the buckle diametrically opposite the longitudinal weld. The amplitude of the buckles varied from 60.3 mm (2.375 in.) to 82.6 mm (3.25 in.)

6.3 Behavior After Buckling

The complete average stress vs. deformation curves including the post-buckling range are shown in Fig. 9. The first portions of these curves are also shown in Fig. 5 to a larger scale. The prebuckling loading and the post-buckling unloading parts of the deformation curve for specimen P9 are noticeably flatter than for specimen P8. This is the result of the twice as great yield stress of P9 used in nondimensionalizing the load. The curves show that following initial buckling, there was an immediate reduction in stress. After the reduction in stress, the stress stabilized at 0.38 F_y for specimen P8 and 0.23 F_y for specimen P9. The increase in axial deformation between initial buckling and stabilization of the stress was 3.26 mm (0.128 in.) for specimen P8 and 14.06 mm (0.553 in.) for specimen P9. After the reduction in stress, the stress gradually decreased and then levelled off.

Specimen P8 is shown at the conclusion of the test in Fig. 10. The lobular buckles which had initially developed both along the transverse weld and adjacent to the bottom of the specimen increased in amplitude and then folded over on themselves. As the specimen continued to deform axially under load, the corners of the lobular buckles, shown in Fig. 11, contacted the surface of the folded section of buckles beneath them. The contact caused a slight increase in the average stress,

approximately 1% F_y, between the axial deformations of 0.175 m (6.9 in.) and 0.20 m (7.93 in.). Then, the corners of the lobes sheared through the specimen wall and the stress gradually decreased until the test was terminated due to excessive deformations at the bottom of the specimen.

Specimen P9 is shown after testing in Fig. 12. Its overall post-buckling behavior was similar to that of specimen P8. The initial buckles which formed at the top of the specimen increased in amplitude and then folded over on themselves. As the specimen continued to deform axially, the corners of the lobular buckles, as shown in Fig. 13, contacted the folded section of buckle above them with essentially no change in the stress. At an axial deformation of approximately 0.114 m (4.5 in.), the corner lobes began punching through the specimen wall and a crack, shown in Fig. 14, developed in the specimen wall adjacent to the inclined section of the buckle between grid lines 7 and 8. In addition, cracks developed along the fold between the inclined surfaces of the buckles as shown in Fig. 15. To prevent contact between the corner lobes and the machine head, the test was terminated after the specimen had been shortened by 0.156 m (6.7 in.).

7. TEST RESULTS

7.1 Comparison with Design Curves and Previous Lehigh Tests

The local buckling test points for specimens P8 and P9 are shown in Fig. 16 by hollow slashed circles together with the test points and design curves of Fig. 1. The test point for specimen P8, which was made from 345 MPa (50 ksi) steel, falls along a smooth curve formed by the previous Lehigh test points, P1 to P7, thus indicating a consistent relationship between the buckling stress and parameter α for 345 MPa (50 ksi) steels. However, the test point for specimen P9 is significantly higher than this imaginary curve.

All the Lehigh test points lie above the design curves shown in the figure, including the AISI and API curves which are recommended for the design of fabricated tubular members in this country. Therefore, it can be concluded that for both nominal 345 MPa (50 ksi) and 690 MPa (100 ksi) steel, the present design curves are conservative.

7.2 Effect of Transverse Weld

The test point for specimen P8, shown in Fig. 16, lies very close to the test point for specimen P6 from which it was made. Since the only essential difference between the two specimens was that specimen P8 had a transverse weld located at midheight, it can be concluded that the transverse weld had no apparent effect on the intensity of the buckling stress.

7.3 Effect of Higher Yield Stress

The local buckling test point for specimen P9, shown in Fig. 16, is significantly higher than the imaginary curve formed by the Lehigh 345 MPa (50 ksi) test points. Since the principal difference of specimen P9 from the other Lehigh specimens was that it had a nominal yield stress twice the value of the other specimens, the higher test value indicates that the yield stress apparently has a different effect on the local buckling stress than is reflected by parameter α.

7.4 Behavior at Buckling and in Post-Buckling Range

The maximum stress attained in a short tubular column is limited by the local buckling stress. At the buckling stress, there is an immediate reduction in load carrying capacity which then gradually levels off to approximately 0.1 F_y. The post buckling strength was approximately 0.11 F_y for specimen P8 and 0.07 F_y for specimen P9, a reduction in strength of 87% and 92%, respectively.

In the post-buckling range, the tubular column dissipates a large amount of energy. The amount of energy dissipated, equal to the area under the average stress vs. deformation curve in the post-buckling range as shown in Fig. 9, appears to be relatively constant for both specimens P8 and P9.

7.5 Effect of Initial Imperfections

The maximum out-of-straightness value of specimen P8 was approximately 6 times greater than the maximum out of straightness value of

specimen P6 from which it was made. Since the buckling stress was essentially the same for both specimens P6 and P8, it can be concluded that the initial geometric imperfections appear to have no significant effect on the intensity of the buckling stress.

A definite correlation between initial imperfections and the location of initial buckling was observed in specimen P8. It appears that the out-of-straightness of the specimen wall along the transverse weld, due to misalignment of the wall above and below the weld, invited buckling along the weld. Since the initial imperfections did not lower the buckling stress of the specimen, this test supports the conclusion made in Ref. 5 that inelastic local buckling intensity relatively insensitive to initial imperfections.

7.6 Prebuckling and Post-Buckling Lateral Deformations of Specimen P9

The pattern of lateral deformations of the wall of specimen P9 was determined for a number of load levels to study the influence of the pattern on the shape and location of the local buckles. The initial and subsequent deformation patterns were computed from test measurements with respect to an ideal cylindrical surface which was used as a reference. The computational procedure is described in Appendix A.

The location of measurement points is shown in Fig. 17. For the purpose of presentation, the specimen is envisioned to have been cut along the longitudinal weld and laid out flat. Thus, the left and right borders of the rectangle in Fig. 17 designate the longitudinal weld. The ordinate is the vertical height of the specimen measured from the

bottom and the abscissa is the circumferencial distance from the longitudinal weld. The intersections of the interior horizontal and vertical lines designate the points of displacement measurements. The measurements were used to generate and plot contour lines by means of a computer.

Figure 18 shows the lateral deformations of specimen P9 at the initial load of 89 kN (20 kips). Figures 19 through 21 show the lateral deformations at the loads of 1780 kN (400 kips), 8896 kN (2000 kips) and 15568 kN (3500 kips) which correspond respectively to 10%, 50% and 87% of the critical buckling load. The contour lines are plotted for each 1.27 mm (0.05 in.). A positive contour value indicates an outward and a negative value an inward lateral deformation. The contour lines adjacent to the longitudinal weld (left and right borders of the rectangle) have been interpolated and are shown by dashed lines.

The pattern of the contour lines was consistent from one load level to another. In the regions adjacent to the longitudinal weld, an outward lateral deformation extended along the weld and decreased in magnitude as the circumferencial distance from the weld increased. The pattern of lateral deformation to the right of the weld (shown on the left side of the figures) gradually changed from an inward deformation at the top of the specimen to an outward deformation at the bottom of the specimen. The pattern of deformation to the left of the weld (shown on the right side of the figures) gradually changed from essentially no deformation at the top of the specimen to a maximum inward lateral deformation at the bottom of the specimen.

Along the longitudinal weld, the outward lateral deformation of the specimen wall increased with an increase in load. Figures 18 and 19 shows an eliptically shaped contour of magnitude 2.5 mm (0.10 in.) along the longitudinal weld. Half of the contour is shown on the right side and half on the left side of the figures. The eliptical contour has a maximum length of 0.97 m (3.2 ft) along the weld and a maximum width across the weld of 0.26 m (0.86 ft). In Figure 20, at the load of 8896 kN (2000 kips), the 2.5 mm eliptical shaped contour increased to 1.18 m (3.9 ft) along the weld and to 0.37 m (1.2 ft) across the weld. Finally, as shown in Fig. 21 at the load of 15568 kN (3500 kips), the maximum outward lateral deformation along the weld increased from 2.5 mm (0.10 in.) to 3.8 mm (0.15 in.).

In the regions to the left and right of the longitidinal weld, the magnitude of the deformation remained constant as the load increased. On the left side of the figures, the deformations at each load were -2.5 mm (-0.10 in.) at the top of the specimen and gradually increased to 2.5 mm (0.10 in.) at the bottom of the specimen. Similarly, on the right side of the figures, the magnitude of the deformations decreased from zero at the top to -5.1 mm (-0.20 in.) at the bottom of the specimen.

Figure 22 shows the cross-sectional shape of the specimen with respect to the ideal cylinder before and after buckling. The ideal cylinder is shown by the light solid line and is labeled "reference cylinder". The dashed line represents the shape of the specimen at the prebuckling load 15568 kN (0.87 P_{cr}), and the heavy solid line represents the shape of the specimen after buckling. The scale used for the

radial displacements from the reference cylinder before buckling is 25 times larger than the scale used for the radial displacements after buckling. This difference in scaling made it possible to show the relative shapes without making the postbuckling deformations excessively distorted.

The shape of the specimen before buckling was determined from the plot of lateral deformations shown in Fig. 21 by interpolating the values along a horizontal line 0.24 m (9.5 in.) from the top of the specimen. The shape of the specimen after buckling was determined from measurements of the distance between a vertical reference line and the buckled specimen wall at the points of peak inward and outward deformation around the circumference.

Several observations can be made regarding the prebuckling and post-buckling lateral deformations of specimen P9. Figures 18 through 21 show that prior to buckling, there was a significant increase in outward lateral deformation along the longitudinal weld. In the remaining portion of the specimen, there was only a very gradual, barely perceptible change in the pattern and magnitude of the deformations up to the last load when measurements were recorded. Figure 22 shows that after buckling there was a large increase in the magnitude and a dramatic change in the pattern of lateral deformations. The pattern before and after buckling followed a consistent trend with inward buckles developing at points of inward lateral deformation in the prebuckled shape. However, at the weld, an inward buckle developed at a point of outward lateral deformation in the prebuckled shape. Hence, no definite

correlation between the pattern of prebuckling lateral deformations and the pattern and location of the buckles could be established.

8. SUMMARY AND CONCLUSIONS

Local buckling tests were conducted on two short tubular specimens fabricated from high-strength steel plate by cold rolling and welding. One specimen, P8, had a transverse weld at midheight and was made from 345 MPa (50 ksi) nominal yield stress steel. The specimen buckled at a stress equal to 0.872 F_y. The other specimen, P9, was made from 690 MPa (100 ksi) nominal yield stress steel and buckled at a stress of 0.912 F_y. The diameter was 1.53 m (60 in.) for both specimens and the wall thickness was 7.26 mm (0.286 in.) for P8 and 6.55 mm (0.258 in.) for P9. The corresponding D/t ratios were 210 and 233.

The principal characteristics of these test specimens which distinguished them from the previous Lehigh test specimens were that one specimen, P8, had a transverse weld but was made of the same yield stress steel, 345 MPa (50 ksi); and the other specimen, P9, was made from a higher yield stress steel, 690 MPa (100 ksi).

The following conclusions can be drawn from the results of these tests:

1. The design rules for local buckling currently recommended by the AISI and the API codes are adequately conservative for tubular members which are fabricated from 345 MPa (50 ksi) steel and fall within the range of the parameters tested.
2. The presence of a transverse weld in a tubular member fabricated from high-strength steel does not appear to affect the intensity of the local buckling stress.

3. The design rules currently recommended for tubular members appear to be more conservative for tubular members fabricated from 690 MPa (100 ksi) steel than from 345 MPa (50 ksi) steel.
4. The initial geometric imperfections of the two specimens tested had no apparent effect on the intensity of the local buckling stress.
5. No definite correlation could be established between the pre-buckling lateral deformations and the pattern and location of the local buckles.

9. TABLES

TABLE 1: SPECIMEN DATA OF LEHIGH TESTS

No.	Steel	Coupon Static F_y (MPa)	Measured OD (m)	Measured t (mm)	Measured L (m)	D/t	α	F/F_y
1	2	3	4	5	6	7	8	9
Previous Tests P1-P7 (Refs. 5 and 6)								
P1	A572 Gr50	319.17	0.717	8.349	2.05	84.85	7.51	0.941
P2	A633 GrD	346.68	0.741	8.037	2.05	92.26	6.42	1.008
P3	A572 Gr50	319.17	1.190	8.349	3.05	141.53	4.50	0.989
P3A	A572 Gr50	319.17	1.190	8.349	2.03	141.53	4.50	1.009
P4	A633 GrD	346.68	1.217	8.037	3.05	151.39	3.88	0.951
P5	A572 Gr50	377.16	1.787	7.165	3.03	248.38	2.17	0.814
P6	A572 Gr50	372.05	1.533	7.262	3.03	210.05	2.60	0.889
P7	A572 Gr50	372.05	1.203	7.262	3.03	164.62	3.32	0.941
Present Tests P8, P9								
P8	A572 Gr50	372.05	1.533	7.262	2.44	210.05	2.60	0.872
P9	A514 Type B	622.76	1.532	6.553	2.44	232.84	1.40	0.912

TABLE 2: MATERIAL PROPERTIES

Specimen	Coupon Number	Coupon Static σ_y (MPa)	Coupon Ultimate σ_u (MPa)	% Elongation	% Reduction of Area
P8	F1	367.17	511.51	21.9	---
	F4	369.03	499.03	24.8	42.6
	F5	369.86	498.68	24.0	42.7
	F6	382.55	513.79	25.5	43.3
P8	Ave.	372.05	505.75	24.0	42.86
P9	T1-1L	629.86	741.24	9.39	35.9
	T1-2L	633.86	723.93	12.56	35.2
	T1-3L	624.00	718.00	9.81	32.5
	T1-4L	603.79	693.03	9.57	33.0
P9	Ave.	622.76	719.05	10.33	34.15

10. FIGURES

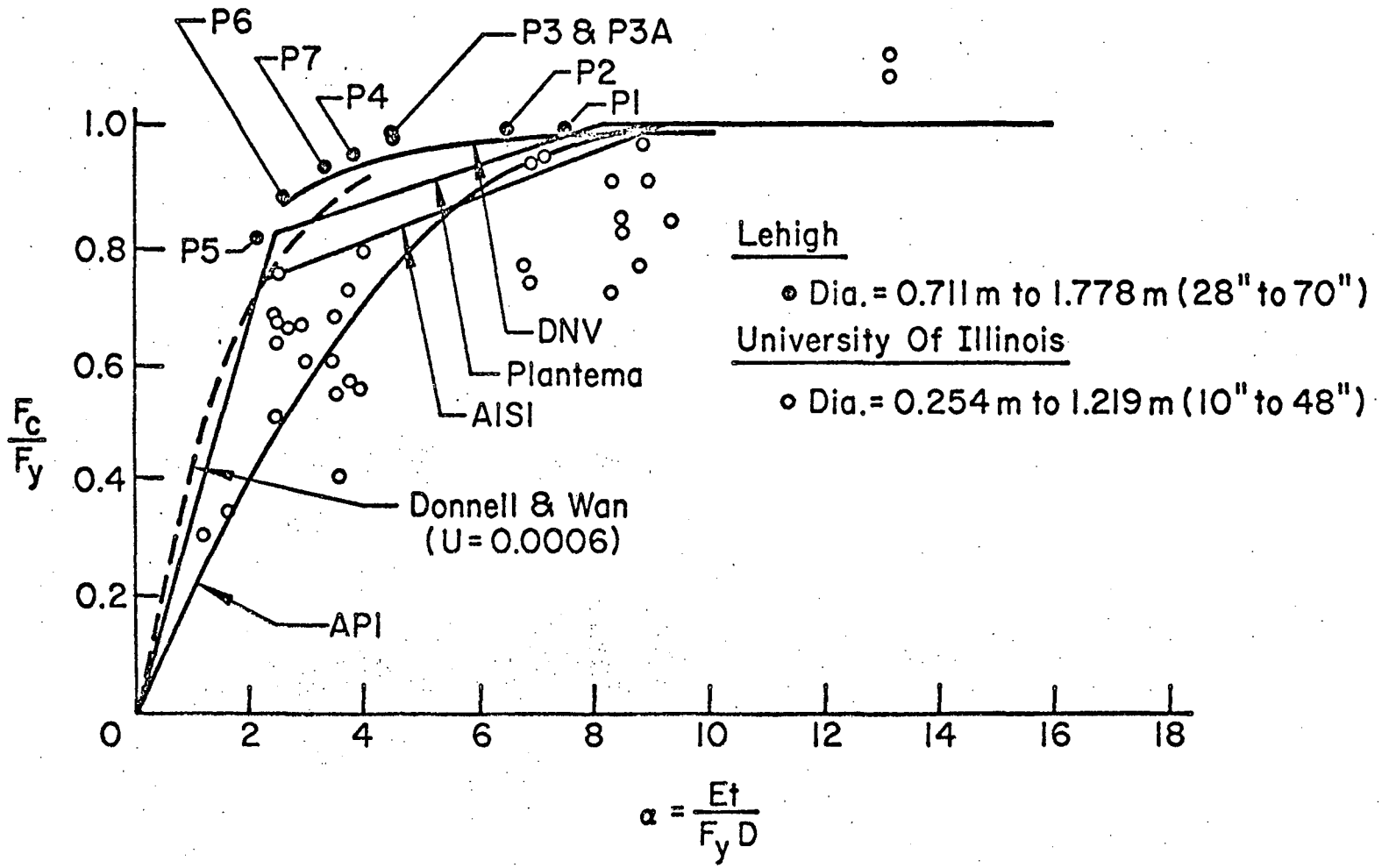

Fig. 1 Design Curves and Previous Test Results for Local Buckling of Tubular Columns

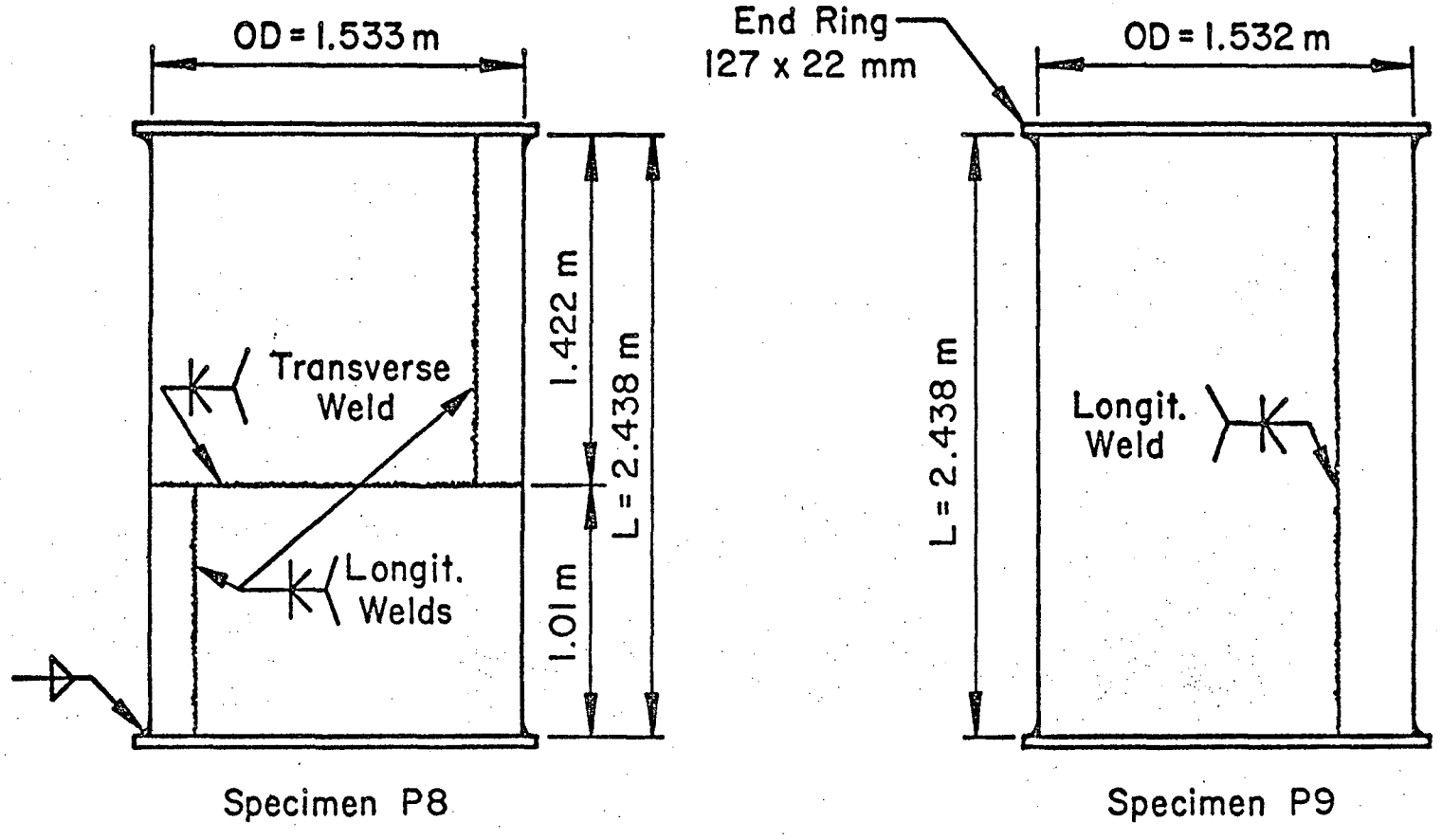

Fig. 2 Test Specimens P8 and P9 and Pertinent Dimensions

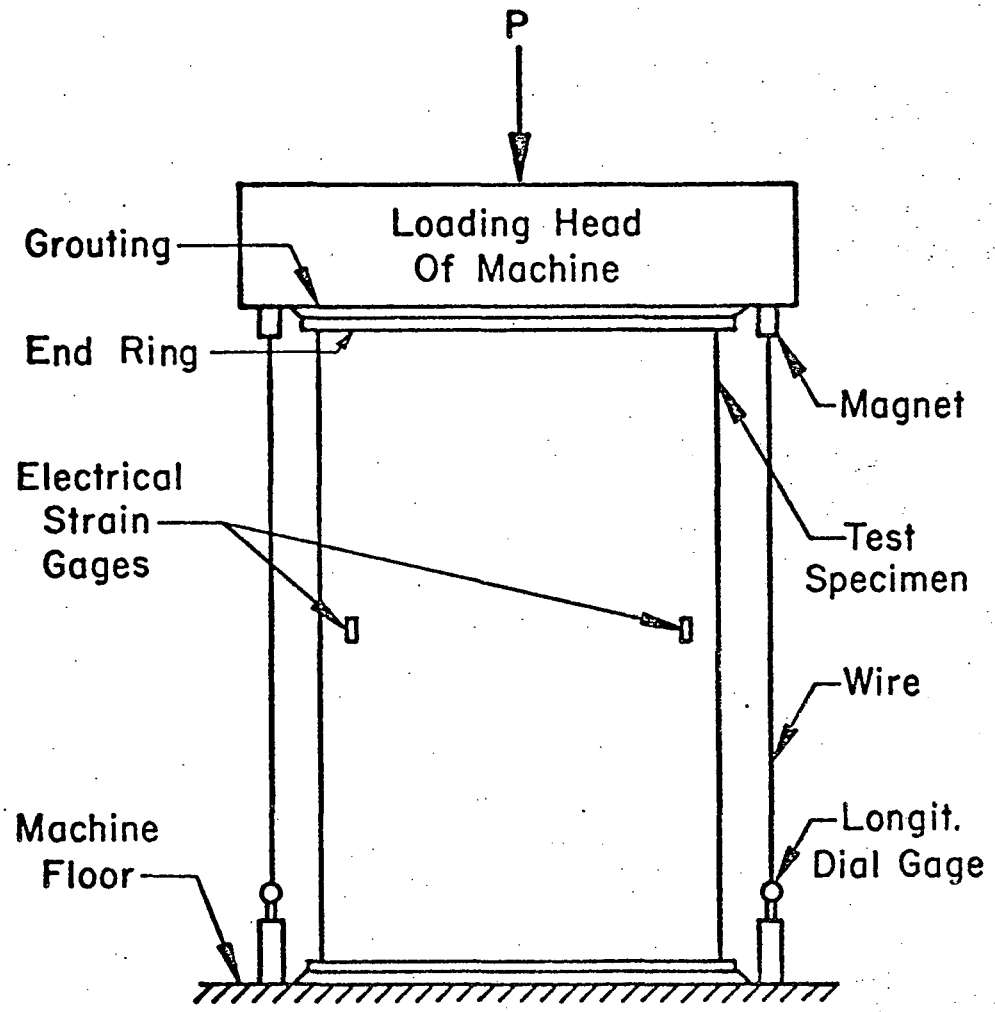

Fig. 3 Test Setup and Instrumentation for Specimens P8 and P9

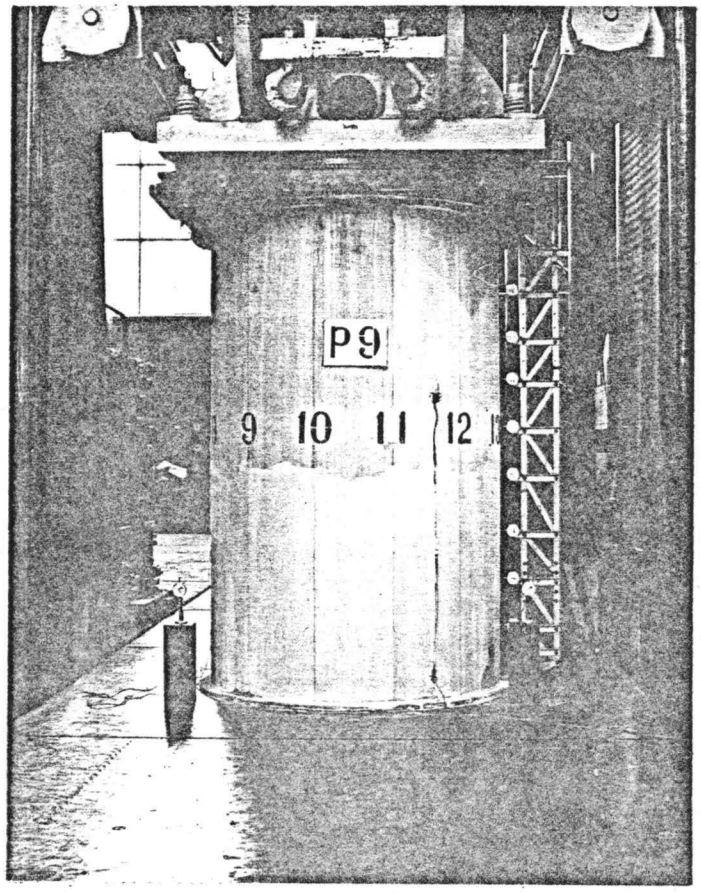

Fig. 4 Specimen P9 Prior to Testing

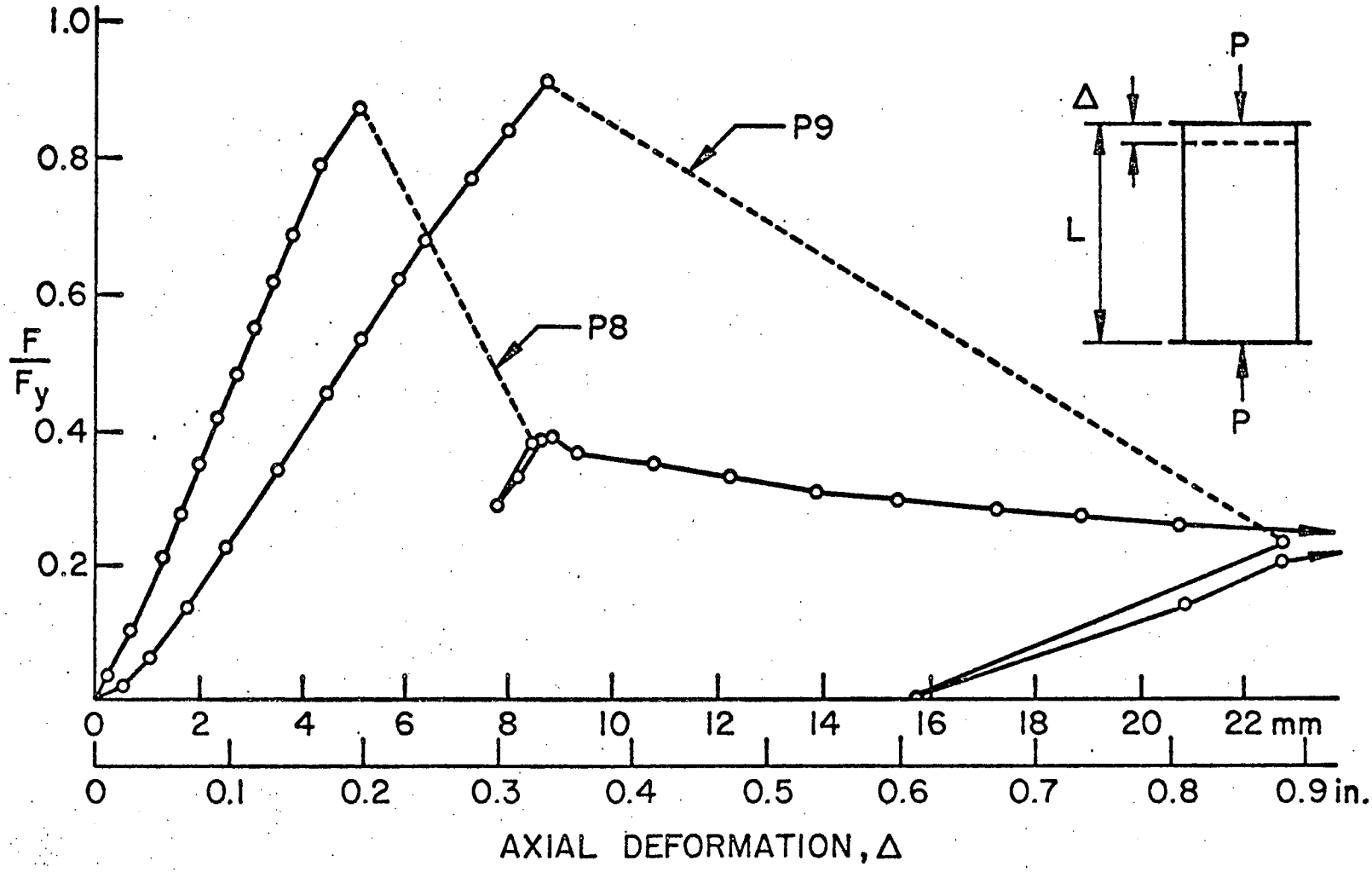

Fig. 5 Average Stress vs. Deformation Behavior of Specimens P8 and P9

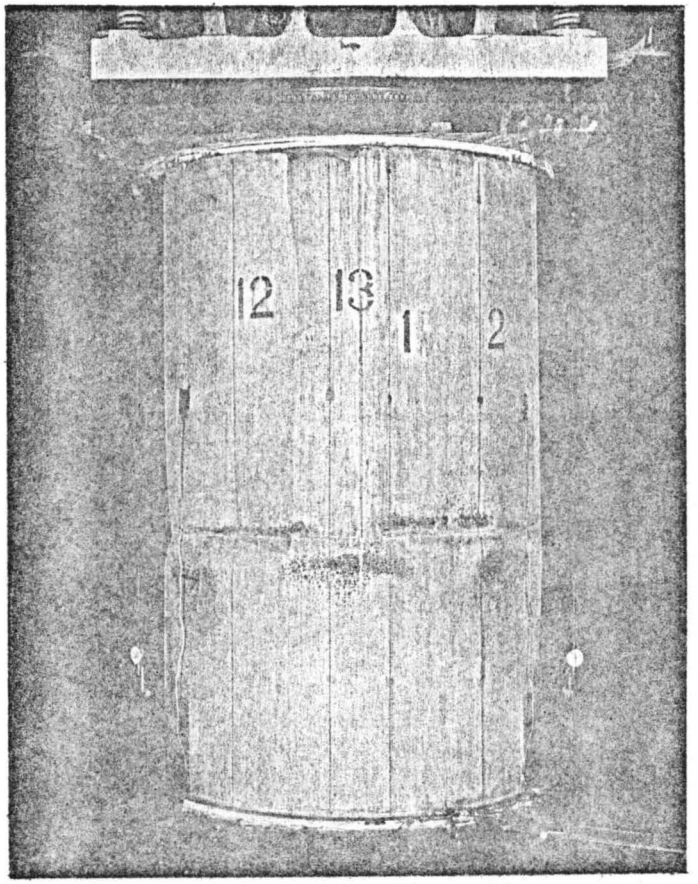

Fig. 6 Initial Lobular Buckles along the Transverse Weld of Specimen P8

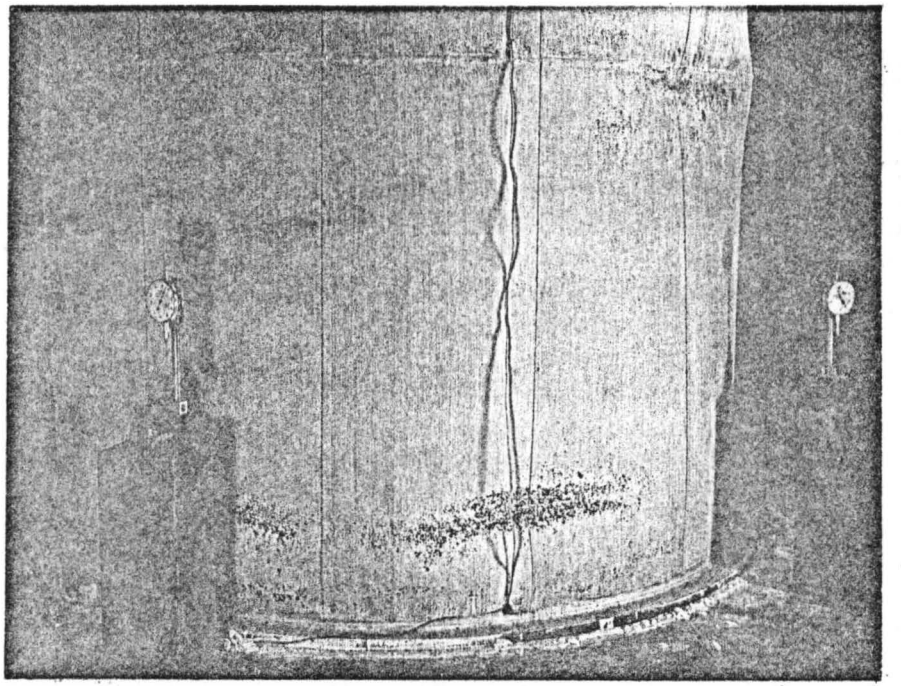

Fig. 7 Initial Lobular Buckles at the Bottom End of Specimen P8

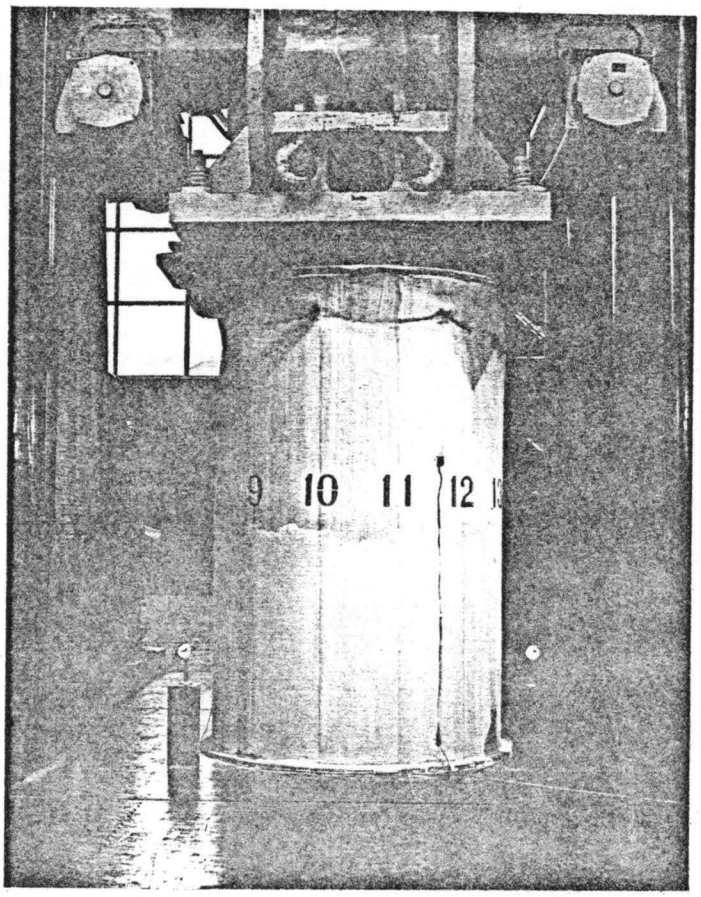

Fig. 8 Specimen P9 after Initial Buckling

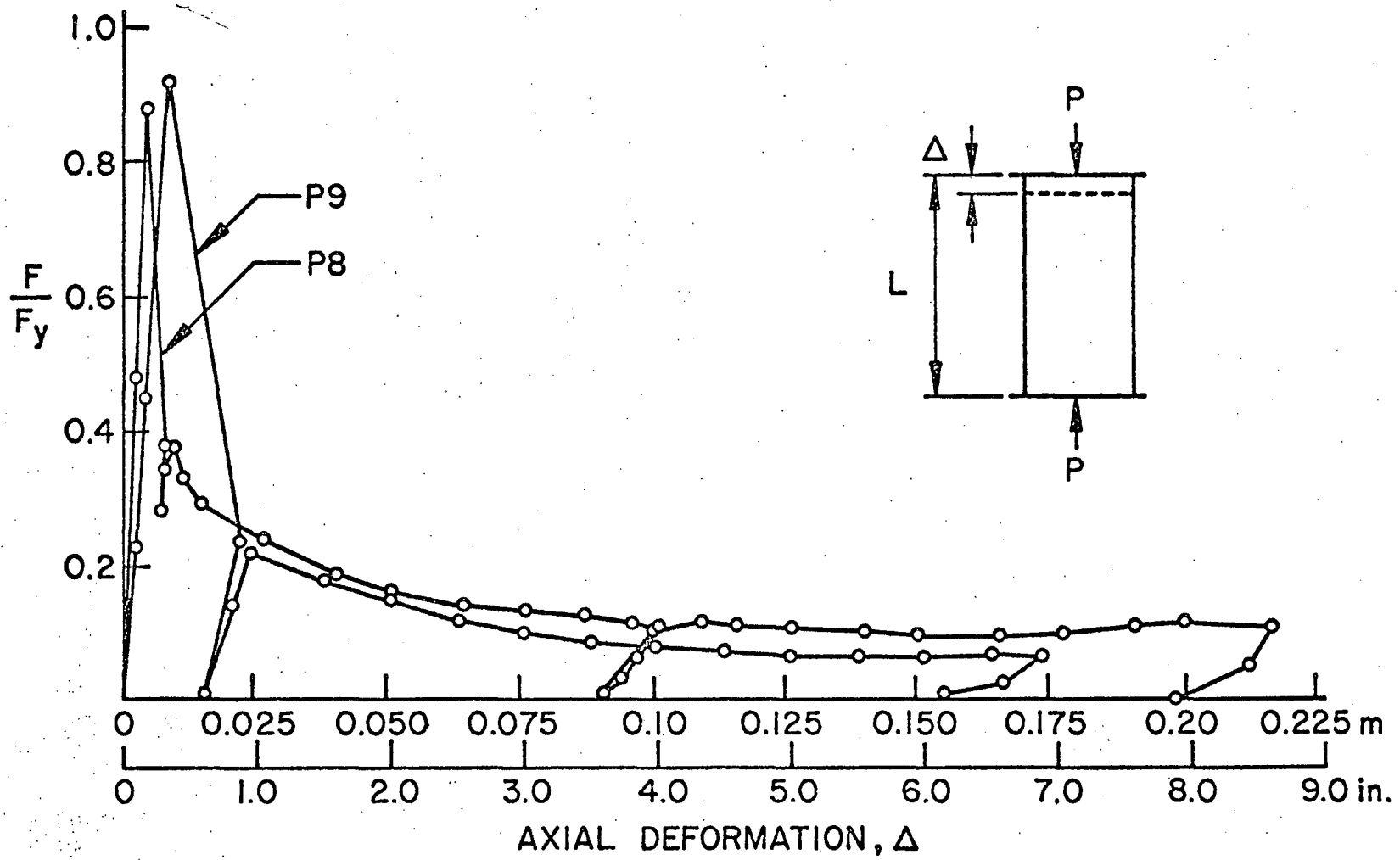

Fig. 9 Comparison of the Average Stress vs. Deformation Behavior for Specimens P8 and P9

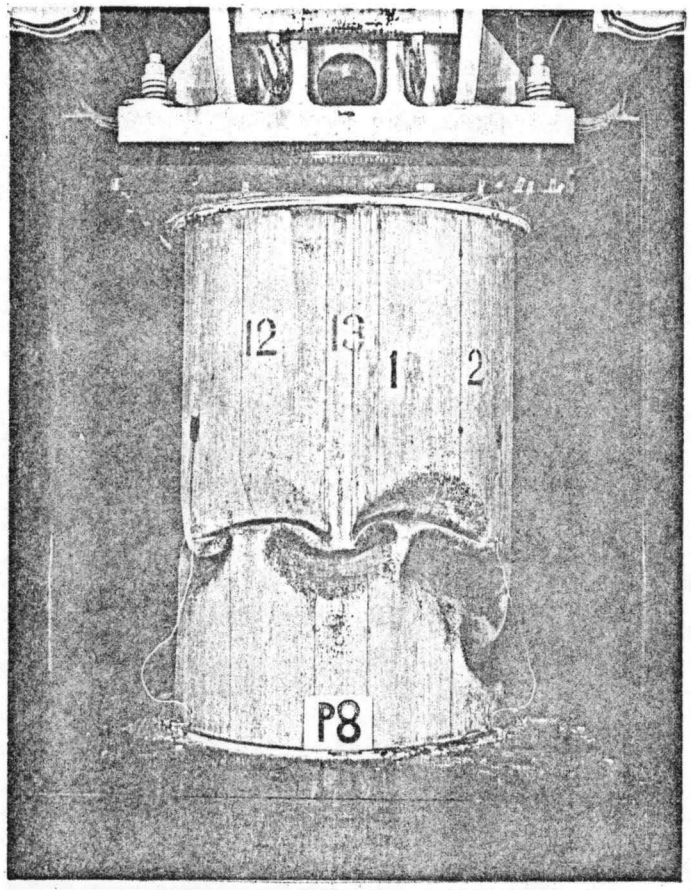

Fig. 10 Specimen P8 after Testing

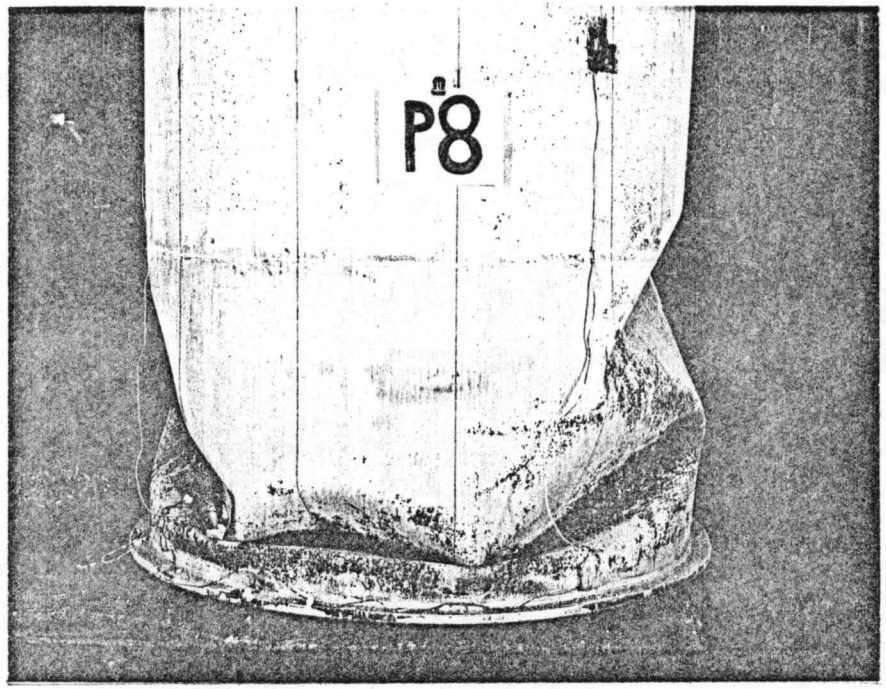

Fig. 11 Corners of the Lobular Buckles at the Bottom of Specimen P8

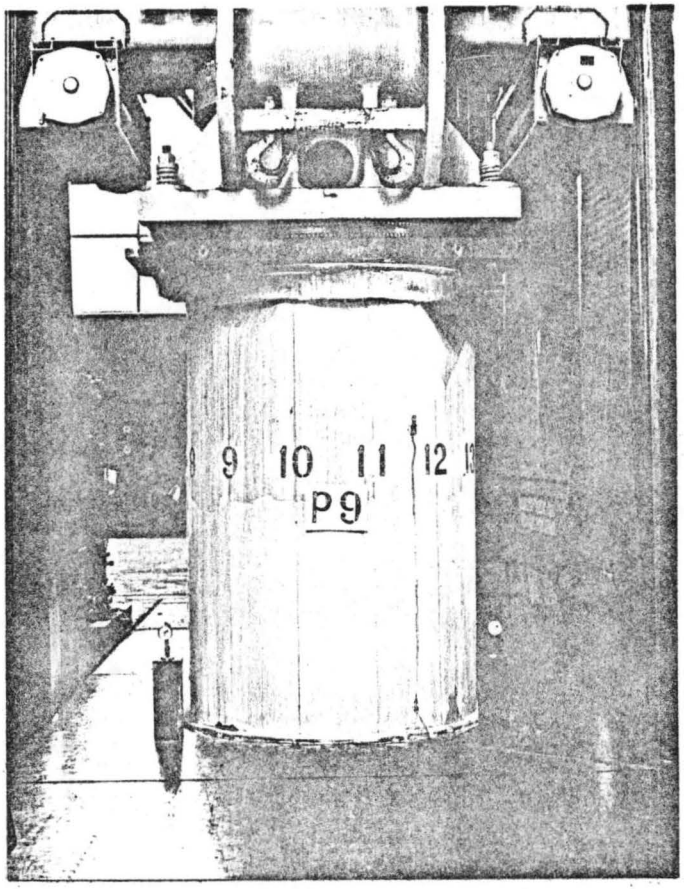

Fig. 12 Specimen P9 after Testing

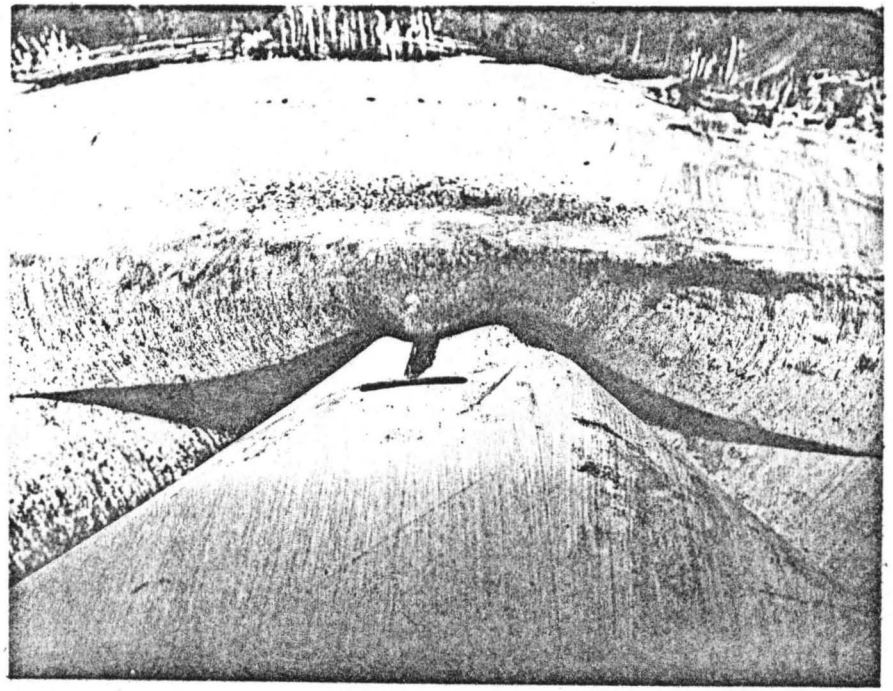

Fig. 13 Corner of a Lobular Buckle Shearing of the Wall of Specimen P9

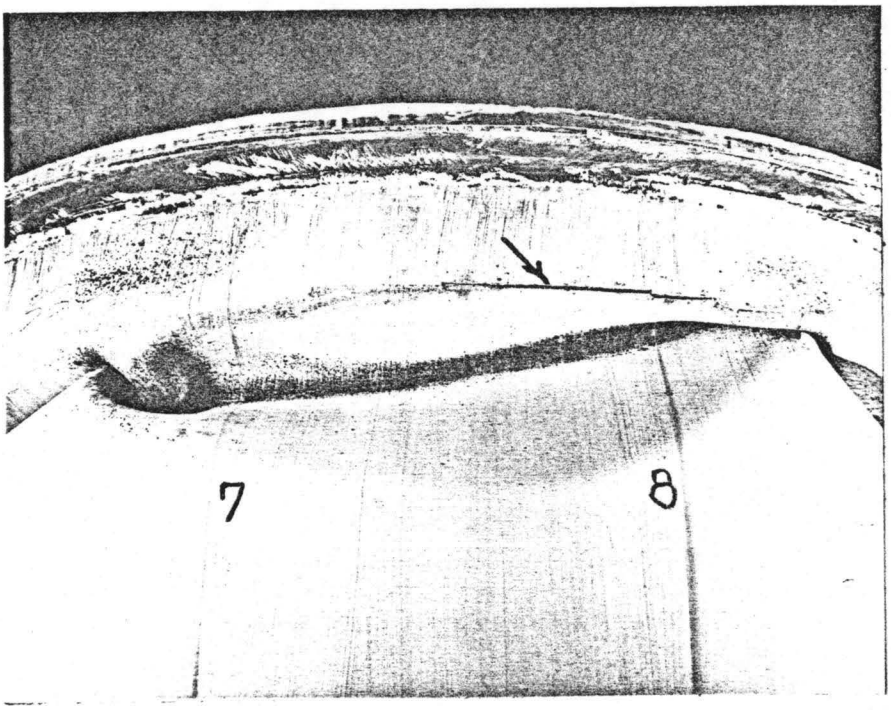

Fig. 14 Crack in the Wall of Specimen P9 adjacent to Inclined Surface of the Buckle

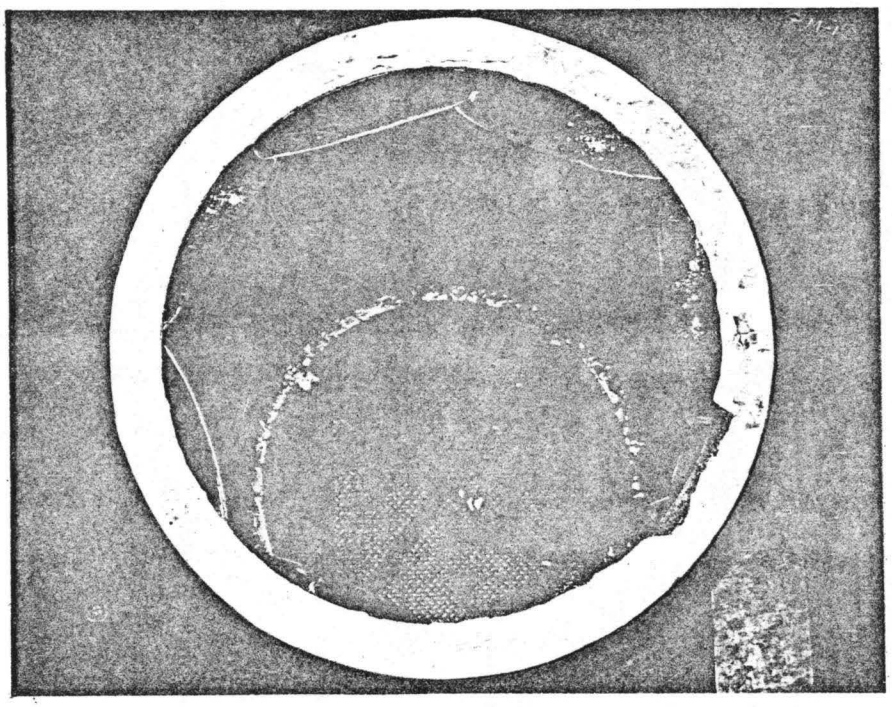

Fig. 15 End View of Specimen P9 Showing Cracks along the Interior Fold of the Buckles

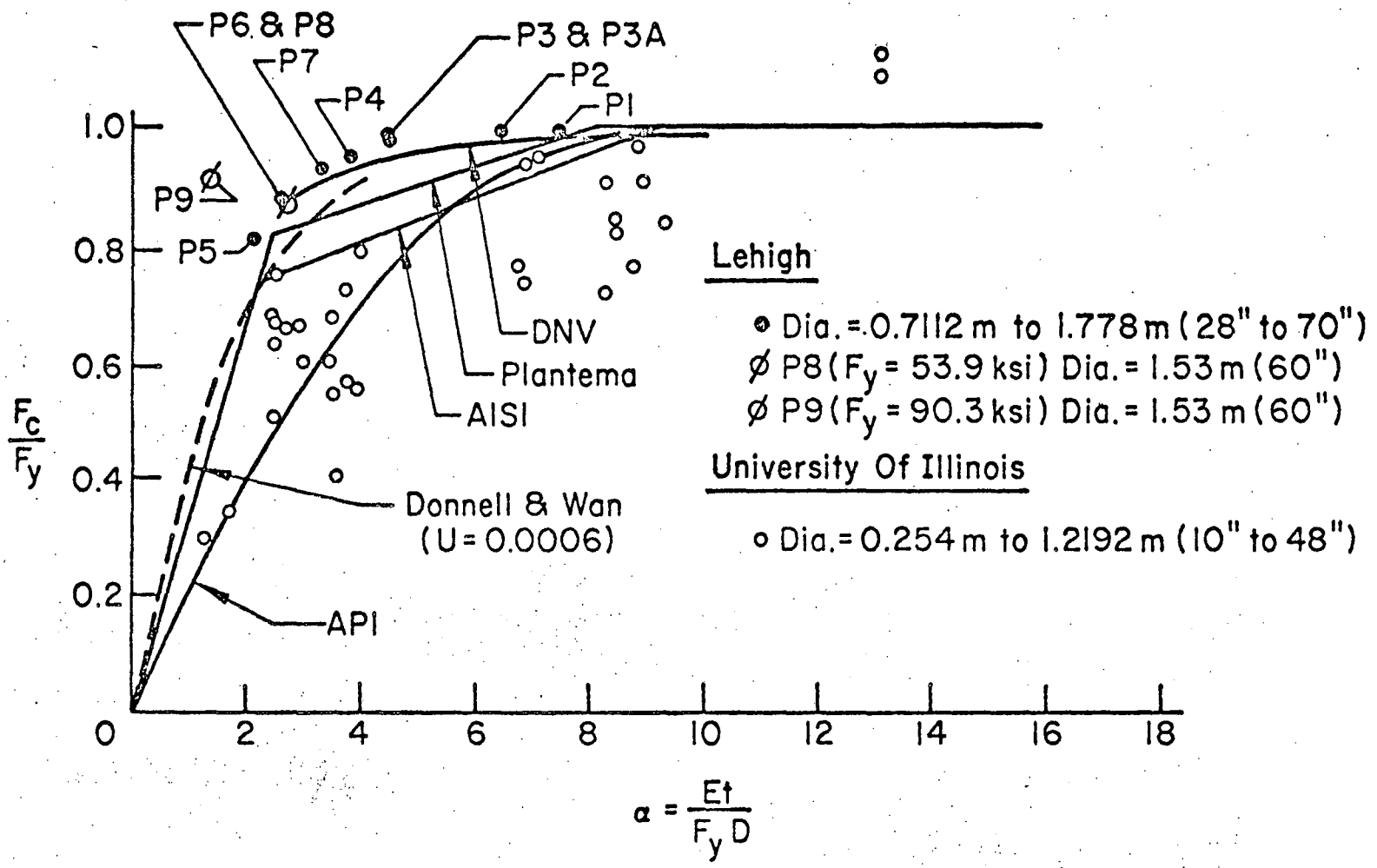

Fig. 16 Test Results of this Study in Comparison with Design Curves and Previous Test Results

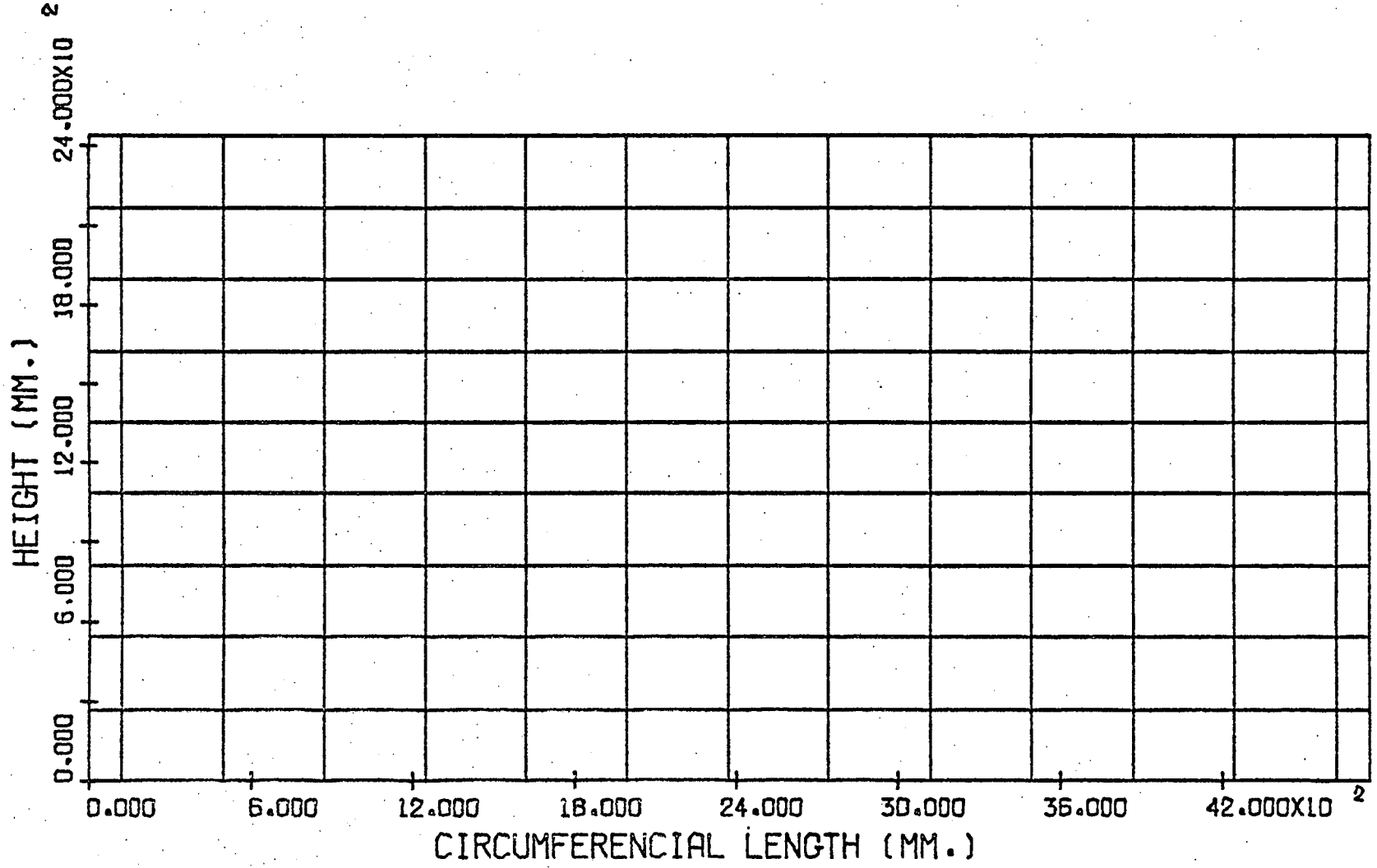

Fig. 17 Location of Measured Lateral Deformations for Specimen P9

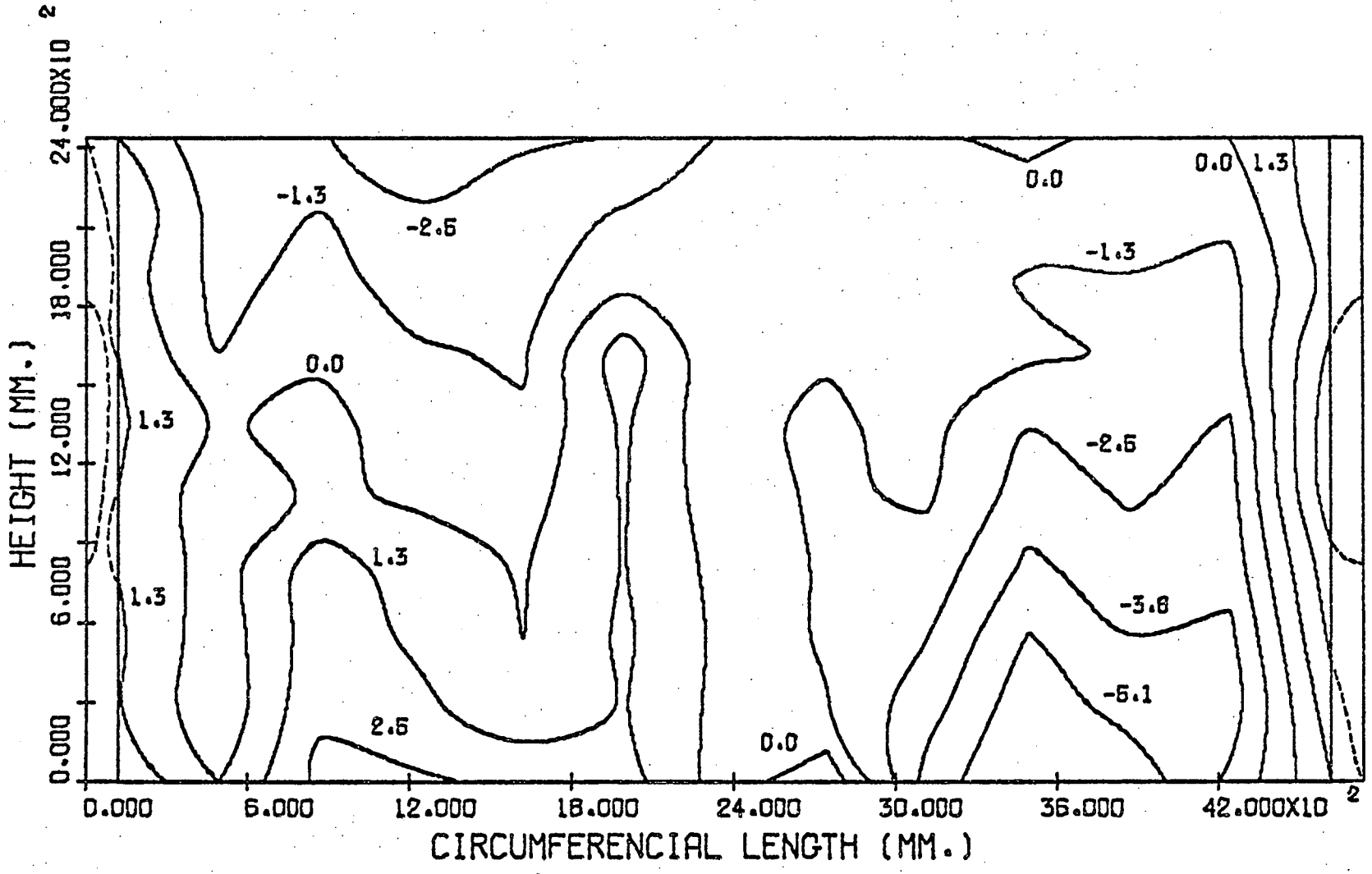

Fig. 18 Contour Plot of Lateral Deformations of Specimen P9 at P = 89kN ($0.005P_{cr}$)

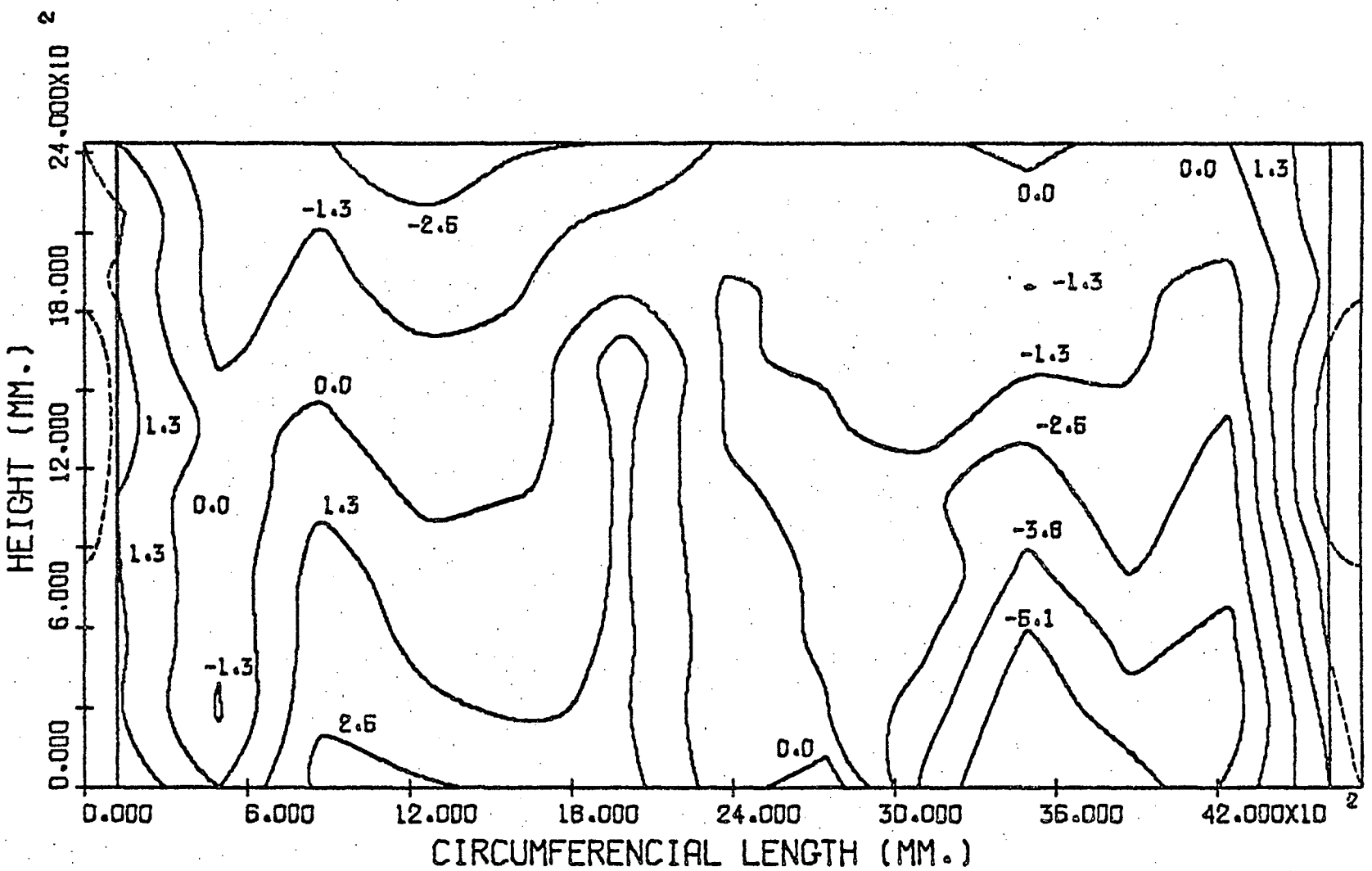

Fig. 19 Contour Plot of Lateral Deformations of Specimen P9 at P = 1780 kN ($0.1P_{cr}$)

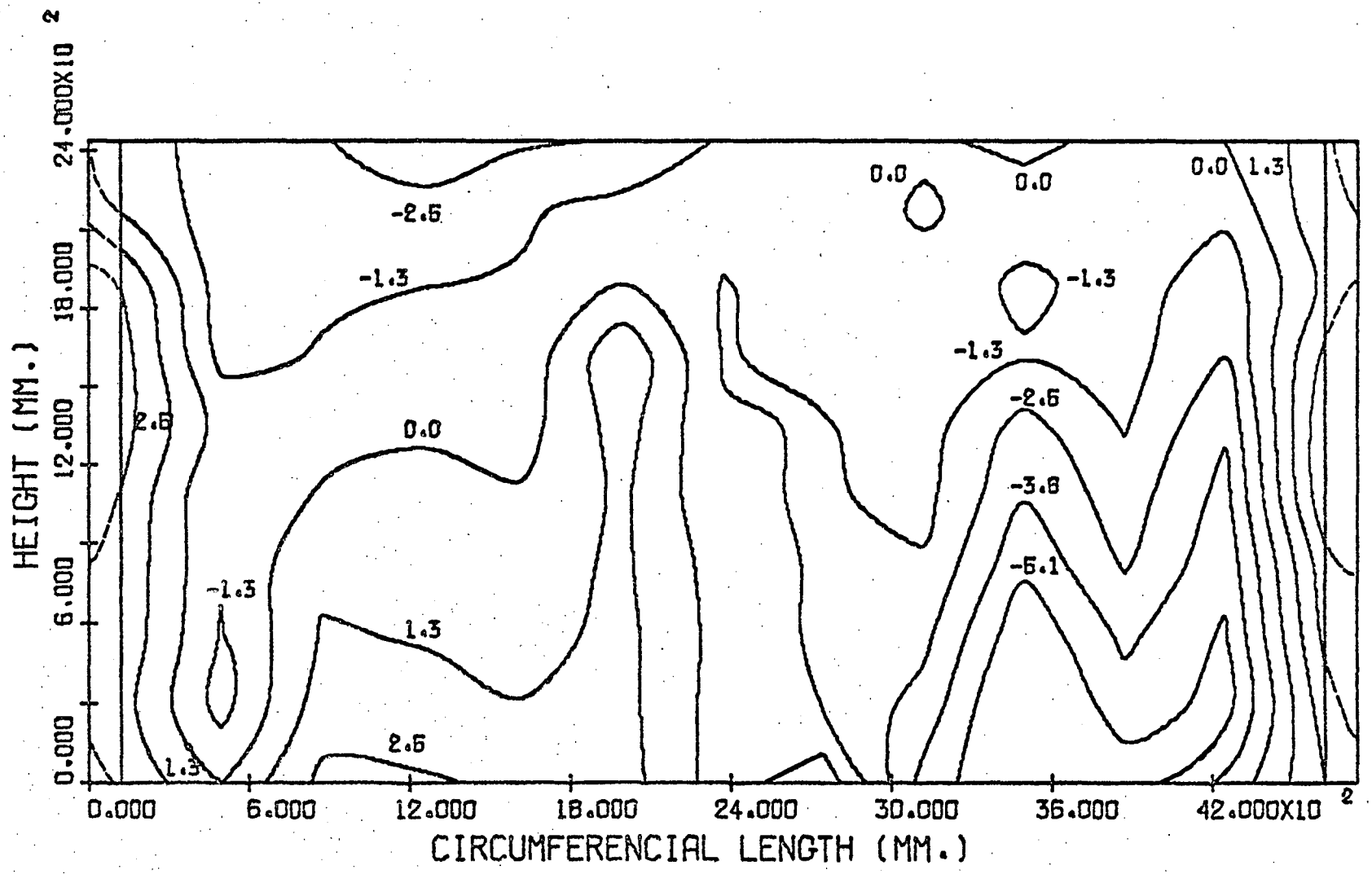

Fig. 20 Contour Plot of Lateral Deformations of Specimen P9 at P = 8896 kN ($0.5P_{cr}$)

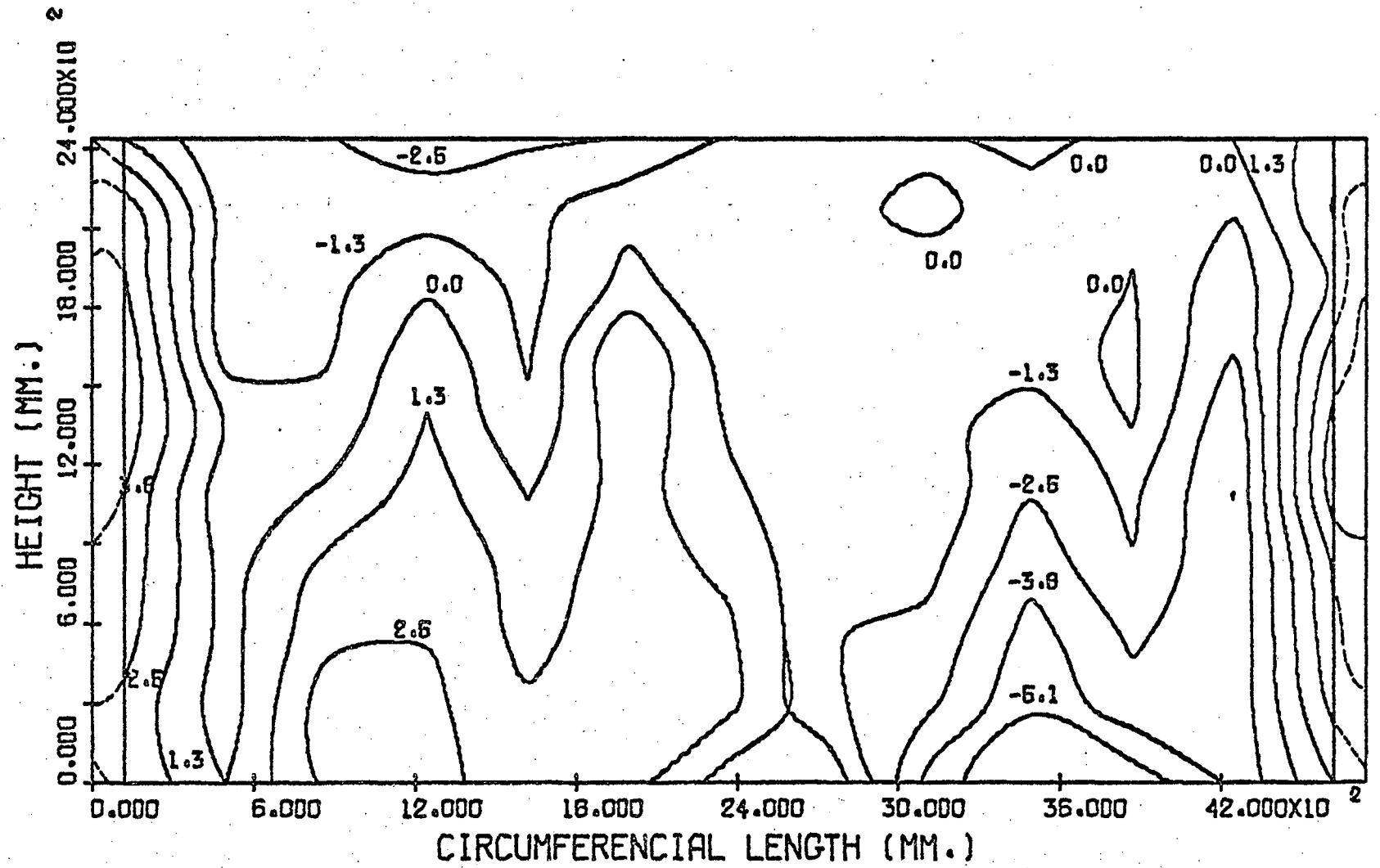

Fig. 21 Contour Plot of Lateral Deformations of Specimen P9 at P = 15568 kN ($0.87P_{cr}$)

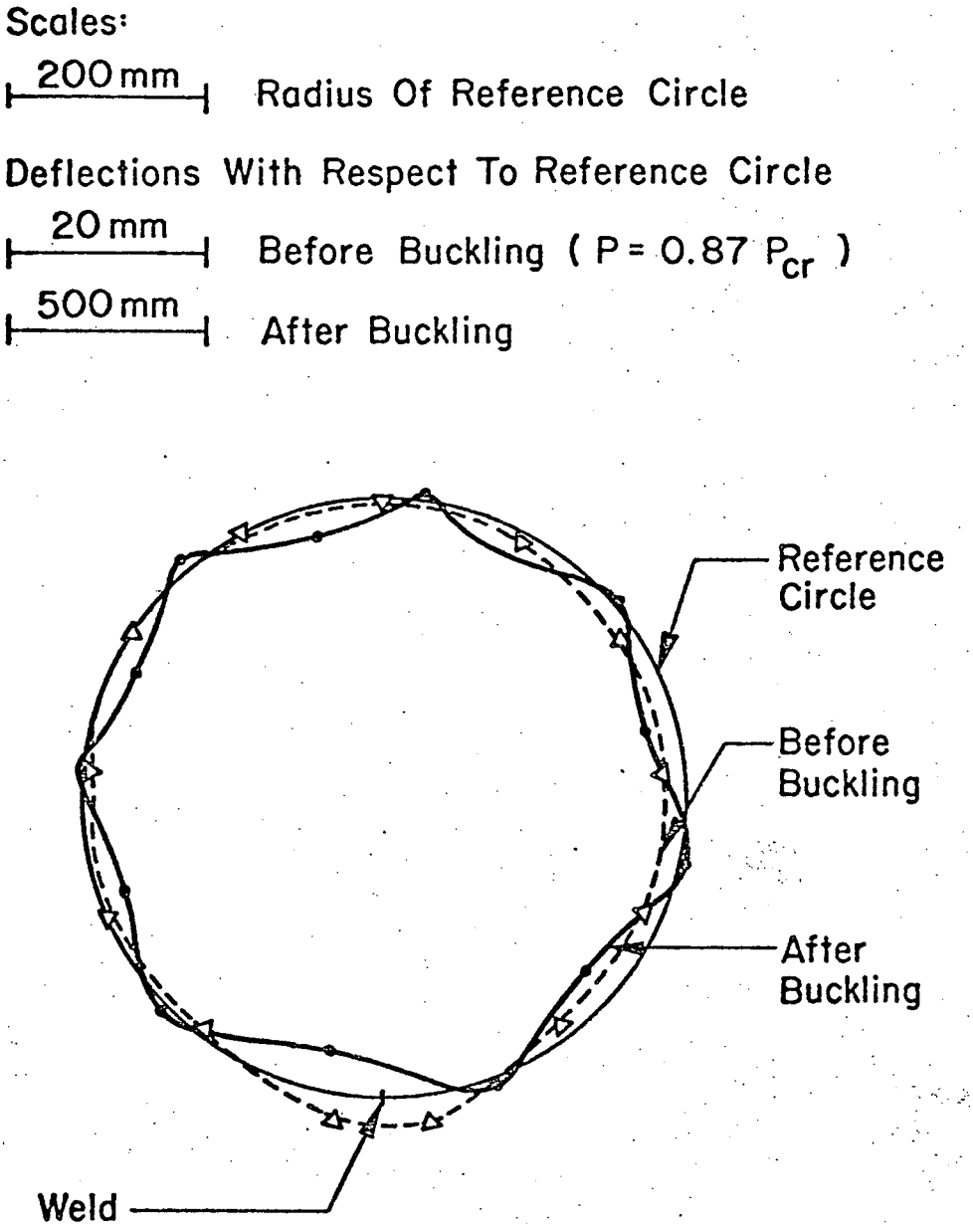

Fig. 22 The Shape before Buckling (P = 0.87 P_{cr}) and after Buckling (P = 0.25 P_{cr}) for Specimen P9

11. REFERENCES

1. American Iron and Steel Institute, "Specification for the Design of Cold-Formed Structural Members," Washington, D. C., 1968, p. 25.

2. American Petroleum Institute, Division of Production, "API Specification 2B," 2nd ed., API Specification for Fabricated Structural Steel Pipe, October 1972.

3. American Society for Testing and Materials, "ASTM Specification E8-69," Annual Book of ASTM Standards, Part 31, pp. 194-213.

4. Donnel, L. H. and Wan, C. C., "Effect of Imperfections on Buckling of Thin Cylinders and Columns under Axial Compression," Journal of Applied Mechanics, Vol. 17, No. 1, March 1950, pp. 73-83.

5. Gunzelman, S. X. and Ostapenko, A., "Local Buckling Tests on Three Steel Large-Diameter Tubular Columns," Fritz Engineering Laboratory Report No. 406.7, Lehigh University, June 1977.

6. Ostapenko, A. and Gunzelman, S. X., "Local Buckling of Tubular Steel Columns," Proceedings, Methods of Structural Analysis, Vol. II, ASCE, New York, N. Y., 1976, pp. 549-568.

7. Plantema, F. J., "Collapsing Stress of Circular Cylinders and Round Tubes," National Luchtraat Laboratorium, Amsterdam, Netherlands, Report S.280, 1946.

8. "Rules for the Design, Construction, and Inspection of Fixed Offshore Structures," Det Norske Veritas, Oslo, 1974.

9. Wilson, W. M. and Newmark, N. M., "The Strength of Thin Cylindrical Shells as Columns," Bulletin No. 255, Engineering Experiment Station, University of Illinois, February 1933.

10. Wilson, W. M., "Tests of Steel Columns, Thin Cylindrical Shells, Laced Columns, Angles," Bulletin No. 292, Engineering Experiment Station, University of Illinois, April 1937.

12. APPENDICES

APPENDIX A: Method of Computing Lateral Deformations

Lateral deformations of the specimen wall were computed with respect to an ideal cylinder used as a reference. The procedure used consisted of first establishing the geometry at each end of the specimen. Next, each end of the reference cylinder, first the bottom and then the top, was located within the corrdsponding end of the specimen. Then, the offsets between the ends of the reference cylinder and the specimen ends at each grid line location were calculated. Finally, the lateral deformations between the ideal cylinder and the specimen wall were computed along each grid line.

The geometry of the specimen ends was determined before the test with the specimen setting outside the testing machine. First, a reference circle approximately 100 mm larger than the diameter of the end rings was drawn on the floor. The specimen, bottom end down, was placed within the circle. Then, at each grid line and at the location diametrically opposite each grid line, the radial distance between the reference circle and the specimen wall was measured. Next, the circumferencial distance between the individual grid lines was measured. The specimen was then turned over and these measurements were taken for the top end of the specimen.

Using these measurements, the diameter through each grid line location and the polar coordinates of each grid line location were computed for the ends of the specimen. The radial coordinate for each grid line location was computed by subtracting the radial distance between the specimen wall and the reference circle from the radius of the

reference circle. The angular coordinate for each grid line was computed with respect to grid line No. 1 using the measured circumferencial distances between the individual grid lines.

After transforming the polar coordinates of each point to rectangular coordinates, each end of the reference cylinder was located within the corresponding end of the specimen. The radius of the reference cylinder was computed from the average of the circumferences measured at the ends of the specimen. The ends of the reference cylinder were located within each end of the specimen so that the reference cylinder passed through the grid line locations on each side of the grid line location corresponding to the largest diameter.

After locating the reference cylinder within the specimen, the offsets between the reference cylinder and the specimen ends at each grid line location were computed.

The lateral deformation of the specimen wall with respect to the reference cylinder was computed at eight locations along each grid line from the original measurements with the dial gage rig taken together with the offsets previously computed at the ends of the specimen. Using the dial gage rig measurements, the lateral offsets a_{ij}, where i designated the grid line location and j the vertical location, were computed between the specimen wall and a straight line passing through the ends of the specimen. Then, the lateral offsets b_{ij} were computed between the reference cylinder and the straight line passing through the ends of the specimen. Finally, the lateral deformation of the specimen wall

with respect to the reference cylinder at each location was computed as the algebraic sum of the two contributions ($a_{ij} + b_{ij}$).

It was assumed in the analyses that the geometry of the ends of the specimens remained constant throughout the test. Therefore, for each load level, only the contribution of the lateral offsets a_{ij} were computed along each grid line since the contribution of the lateral offsets b_{ij} were constants through the test.

APPENDIX B: Nomenclature

D = mean diameter of tubular column

E = modulus of elasticity

F = local buckling stress

F_y = yield stress

L = length of tubular column

OD = outside diameter of tubular column

P = axial load

P_{cr} = axial load at buckling

t = wall thickness of tubular column

α = E/F_y (t/D) = nondimensional wall slenderness parameter

Δ = axial shortening of tubular column

13. VITA

Marc A. Marzullo, the son of Pearl and Vito E. Marzullo, was born July 18, 1952, in Lowell, Massachusetts.

He received his primary education in the public school system of Foxborough, Massachusetts and was graduated from Foxborough Senior High School in 1970. His undergraduate education was obtained at Franklin Institute in Boston, Massachusetts where he received an Associate in Engineering Degree in 1973 and at Southeastern Massachusetts University in North Dartmouth, Massachusetts where he received a Bachelor of Science in Civil Engineering with high distinction in 1976.

In August 1976, he was appointed as a Research Assistant and in September 1977, as a Teaching Assistant in the Department of Civil Engineering, Lehigh University, Bethlehem, Pennsylvania. In January 1978, he was awarded the Master of Science Degree in Civil Engineering, with a major in structures.